J. Fluid Mech. (1985), *vol.* 159, *pp.* 105–130
Printed in Great Britain

Measurements in the turbulent boundary layer on an 'infinite' swept wing

By P. BRADSHAW AND N. S. PONTIKOS
Department of Aeronautics, Imperial College, London SW7 2BY, England

(Received 12 November 1984)

The results are presented of turbulence measurements on an 'infinite' swept wing, simulated by a duct attached to a blower tunnel. The configuration is close to that used at the Netherlands NLR except that the boundary layer does not quite separate. The measurements include triple products, and a balance of the transport equation for turbulent energy is presented. The results confirm the NLR finding of a significant decrease in the magnitude of shear stress compared with an equivalent two-dimensional boundary layer: this is evidently the effect of crossflow on large eddies that have initially developed in a two-dimensional boundary layer. This unexpected effect of three-dimensionality is at least as important in prediction of real-life flows as the better-known lag between the direction of the shear stress and that of the mean-velocity gradient. Tentative suggestions for modelling the reduction in shear-stress magnitude are advanced.

1. Introduction

Most current calculation methods for three-dimensional ('3D') boundary layers are formal, rotationally invariant extensions of two-dimensional methods, in which the 'spanwise' component of shear stress – using aeronautical terminology for convenience – is modelled in the same way as the chordwise component. A typical 3D flow is that over a swept-back wing, with fairly small pressure gradients over the front portion, followed by a positive chordwise (axial) pressure gradient with isobars roughly coincident with the swept-back generators of the wing surface, so that the negative pressure gradient in the spanwise direction (normal to the aircraft axis) deflects the flow towards the wingtip.

It has been accepted for many years that if an initially two-dimensional boundary layer is driven into three-dimensionality by a pressure gradient, the direction of the shear-stress vector (that is, the direction of the two-component vector seen in plan view, whose components are the 'chordwise', or axial, and 'spanwise', or lateral, components of shear stress) lags behind the direction of the velocity-gradient vector, whose components are the gradients, normal to the surface, of the chordwise and spanwise velocity components. In the axes used below, e.g. figure 1, in which x is the chordwise and z the spanwise direction, with y as the direction normal to the surface, this implies

$$\frac{\overline{vw}}{\overline{uv}} < \left(\frac{\mathrm{d}W}{\mathrm{d}y}\right) \Big/ \left(\frac{\mathrm{d}U}{\mathrm{d}y}\right). \tag{1}$$

Note that, if the effect of three-dimensionality is to produce a positive W-component mean velocity, then $\mathrm{d}W/\mathrm{d}y$ will be negative over most of the boundary layer, because a given pressure gradient deflects the slow-moving fluid within the boundary layer

more than the faster-moving free stream. The generation of this 'secondary flow' is quasi-inviscid (Hawthorne 1951; Squire & Winter 1951; Johnston 1960; Goldberg & Reshotko 1984), but near the surface the no-slip boundary condition enforces a region of positive $\mathrm{d}W/\mathrm{d}y$ via the gradient of the shear stress in the (y,z)-plane, $-\mathrm{d}vw/\mathrm{d}y$.

Van den Berg *et al.* (1975) reported mean-flow measurements at the Netherlands NLR on a model representing a 35° swept, 'infinite' (very high aspect ratio) wing; turbulence measurements in the same rig were reported by Elsenaar & Boelsma (1974). By the time of Euromech 60 (and the accompanying comparison of calculation methods known as the 'Trondheim Trials'; see East 1975 and Fannelop & Krogstad 1975) it was clear that there were significant discrepancies between the NLR measurements – the only data for a 3D boundary layer in prolonged adverse pressure gradient – and the available calculation methods. Methods based on an isotropic eddy viscosity cannot produce a lag in shear-stress direction behind the direction of the mean-velocity gradient, which arises because the Reynolds stresses obey partial differential 'transport' equations rather than algebraic formulae. However, even calculation methods based explicitly on the transport equations seem to underestimate the lag. Furthermore, the transport-equation methods presented at the Trondheim trials were also unable to reproduce the decrease in *magnitude* of the shear stress found at the downstream stations in the NLR boundary layer.

To improve the predictions of shear-stress direction (i.e. of the lag angle), Rotta (1979) proposed a generally applicable modification to calculation methods based on a consideration of the direction of the mean-velocity vector. Unfortunately any model that directly uses the mean-velocity vector (as distinct from the velocity-gradient vector) violates the principle of Galilean (translational) invariance. Such a model would, for instance, produce quite different effects in the flow from the stationary to the rotating part of a turbomachine hub according to whether the velocity was measured with respect to the local surface or to some 'fixed' point: more generally, results in a coordinate system fixed to a solid surface will vary according to the velocity difference across the viscous sublayer – that is, according to the Reynolds number, which does not normally appear directly in turbulence models for outer-layer behaviour. Exactly the same objection applies to the various schemes which assign different values to the spanwise and chordwise components of eddy viscosity: the results depend on the axes, and while this may be empirically useful for flows that become three-dimensional after a well-defined two-dimensional history it is not generally acceptable. On the other hand, properly invariant attempts to base model modifications on the difference between the shear-stress direction and the velocity-gradient direction have no effect on eddy-viscosity methods and seem not to have achieved any success when applied to other methods. Therefore we do not discuss models of this type further, although purely empirical modifications to turbulence models can obviously produce good agreement with a small range of data irrespective of physical plausibility. A model which is in principle free from the 'invariance' objection is that of van den Berg (see Fernholz 1982) who considers the pressure–strain term in the Reynolds-stress transport equations directly: however the assumption made for the pressure fluctuation is somewhat crude and difficult to connect with eddy behaviour. Finally, since our interest is in the turbulence structure, we do not need to consider the effects of breakdown of the boundary-layer approximation – specifically, the appearance of a significant normal pressure gradient – on mean-flow predictions.

The present work is an extension of the NLR experiment to include the measurement of triple products of velocity fluctuations, so that all the terms in the Reynolds-stress

transport equations could be obtained by direct measurement or by difference. The curious behaviour of the shear-stress magnitude and of the 'lag angle' must be attributable to the pressure–strain 'redistribution' term in the Reynolds-stress transport equations, but this term is not at present directly measurable and must therefore be deduced by difference. The measurements were made at about the same Reynolds number as the NLR experiments, but used a 0.762×0.127 m (30×5 in.) blower wind tunnel instead of the 3×2 m return-circuit tunnel used at NLR. The mean-velocity and Reynolds-stress measurements essentially confirm the results of the NLR experiment, and it is found that the triple products, like the Reynolds stresses, decrease significantly near the downstream end of the flow. Unlike the NLR flow the present boundary layer does not reach separation: this was a deliberate choice for the first series of experiments to avoid possible unsteadiness in the flow, which may contribute more to the normal stresses than to the shear stresses, thus producing a *spurious* decrease in the ratio of shear stress to turbulent intensity.

Measurements in 3D boundary layers of the type found on swept wings are reviewed by Johnston (1976) and Cebeci (1984): see also the IUTAM conference proceedings edited by Fernholz (1982), especially the paper by van den Berg. In wing boundary layers, the streamwise component of vorticity is nearly equal to $\mathrm{d}W/\mathrm{d}y$ (with y normal to the surface), $\mathrm{d}V/\mathrm{d}z$ being very much smaller. That is, the mean vorticity can be thought of as made up of vortex sheets roughly parallel to the (x, z)-plane, rather than streamwise 'line' vortices with $\mathrm{d}V/\mathrm{d}z$ of the same order as $\mathrm{d}W/\mathrm{d}y$, which occur near wing roots and wing tips and in other 'slender' flows.

In the present paper, our main concern is with the outer layer of the boundary layer: we do not consider the validity of the various forms of the law of the wall that have been suggested for 3D flows (for a review see Pierce, McAllister & Tennant 1983). The effect of the no-slip condition at the surface spreads only rather slowly into the outer part of the boundary layer: therefore the change in shear-stress profile near the wall, which begins when a pressure gradient is applied, is confined to an 'internal layer' within the inner part of the flow. The behaviour of the outer layer in flows like the present one, specifically the departure of turbulence-structure parameters from normal two-dimensional values, is attributable to the addition of a secondary spanwise shear $\mathrm{d}W/\mathrm{d}y$ to the two-dimensional shear $\mathrm{d}U/\mathrm{d}y$ under which the boundary layer initially developed. In practical flows the direction of the mean-shear vector may change continuously all the way from the flow origin, but the effect on turbulence structure will be similar. Also, practical flows may not approximate to 'infinite' swept wings, but there is no serious suggestion that the low values of shear-stress magnitude found in the NLR experiment and in the present results are peculiar to this configuration. Therefore the present results, and deductions from them, should be applicable to any kind of 3D boundary-layer flow, at least in the absence of significant concentrated streamwise vortices.

2. Equipment and techniques

The working-section duct shown in figure 1 was attached to one of the blower tunnels described by Bradshaw (1972). Measurements were made on the floor of the duct, which had a suction slot swept at 35° to create a new boundary-layer origin, simulating the leading edge of a swept wing. A 1 mm trip wire was taped to the floor just behind the slot. A pressure gradient was applied by bending the roof upwards, the generators of the developable roof shape being swept at 35° and remaining horizontal. An infinitely wide rig of this sort would produce infinite-swept-wing

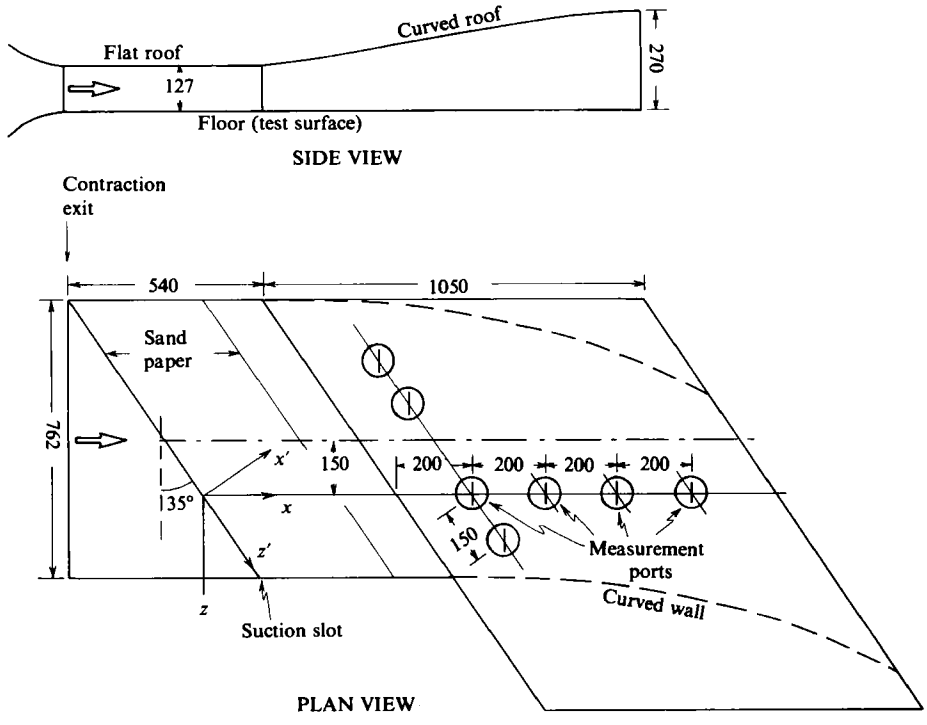

FIGURE 1. Test duct for 762 × 127 mm blower tunnel, simulating 35° swept wing. All dimensions in mm.

conditions, the gradients (but *not* the velocities) along the lines of 35° sweep being zero. In a rig of finite width it is necessary to deflect the sidewalls to follow the streamlines of the inviscid flow or, in practice, to minimize the variation of static pressure along the generators. The approximation to infinite-swept conditions (figure 2*a*) seems to be rather closer than that of the NLR rig, while the final pressure distribution achieved (figure 2*b*) reproduces the streamwise variation of pressure set up in the NLR experiments fairly accurately. The x-direction – along the tunnel axis – will be referred to below as 'axial' and the z-direction as 'cross-stream' or 'lateral': these are the chordwise and spanwise directions of aeronautical terminology, but the latter terms invite confusion with the x'- and z'-axes aligned with the generators (figure 1).

Figure 2(*c*) shows the velocity magnitude at the boundary-layer edge (actually deduced from surface pressures), normalized by the value at the first measurement station: the same figure shows the friction velocity. Figure 2(*d*) shows the angle between the edge velocity and the value at the first measurement station: for a truly infinite swept wing this is uniquely related to the velocity magnitude by the requirement of constant velocity component along the generators. In the present experiments the flow at the initial station was very nearly along the tunnel axis, but in the NLR experiment there was already significant lateral flow at the reference station: this accounts for the rather large difference between the two curves in figure 2(*d*) and for some other differences between the two experiments. The aspect ratio of the present rig is considerably smaller than that of the NLR model, and we

checked that fluid from the 'outside'-wall boundary layer did not travel across the floor as far as any of the measurement stations, which were located nearer the 'inside' wall to avoid this. The boundary layer downstream of the suction slot is thickened by sandpaper on the surface, so the profile shape at the start of the adverse pressure gradient is only roughly representative of a flat-plate boundary layer and has a 'wake parameter' as large as 0.87 compared with the equilibrium value of about 0.6, although the behaviour of dimensionless turbulence parameters appears to be standard. The initial boundary-layer thickness was kept somewhat smaller than in the NLR experiment, resulting in a smaller dimensionless pressure gradient without separation.

Conventional hot-wire techniques were used, with DISA 55D01 and 55M01 anemometers and home-made cross-wire probes using 5 μm platinum (Wollaston) wires. The active length of the wires was 1 mm, with approximately 1 mm sleeves. Wire angles were nominally 45° but were not measured directly, the measured yaw calibrations being fitted by a 'cosine' law to give an effective wire angle. This calibration fit, if accurate, implies that the probe resolves velocity components along and perpendicular to its own axis, rather than relative to the local-mean-flow direction. Therefore, providing that crossflow angles are not too large, it is not necessary to point the probe directly into the flow, nor is it necessary to make corrections for crossflow angle or incidence as in the NLR experiments. In fact, all the measurements were made with the probe pointing along the tunnel axis, crossflow angles in the outer part of the boundary layer being less than 10° even at the station furthest downstream. As in the NLR experiments and our own previous work, statistics involving v- and w-component-velocity fluctuations together were obtained by rotating the cross-wire probe through angles of plus and minus 45° about its own axis, so that it responded to $(v+w)/\sqrt{2}$ or $(v-w)/\sqrt{2}$ instead of simply to v or w: all required Reynolds stresses and triple products can be obtained from mean squares or mean cubes of the wire difference signals. The differencing procedure increases error and accounts for some of the scatter in v, w statistics.

All hot-wire fluctuation signals were recorded on analog tape and later transcribed to digital tape for batch processing – including linearization of calibrations – on the College Cyber computers. Data analysis was conventional: the intermittency factor was obtained by declaring the flow at each instant to be 'turbulent' if the numerical values of either the first or the second time derivative of uv, obtained from digitized records by central-difference formulae, exceeded given thresholds. The thresholds were respectively 0.3 times the rectified-mean value of $\mathrm{d}uv/\mathrm{d}t$ and 0.35 times the rectified-mean value of $\mathrm{d}^2uv/\mathrm{d}t^2$, both mean values being averages over the turbulent zones only. Guessed threshold values are read into the program and used for the first few thousand points of digital data, after which the thresholds are based on continuously updated values of the rectified means.

The only novel equipment used during the experiment was the 'surface-fence' surface-shear-stress meter described by Pontikos & Bradshaw (1981) in which two surface fences at right angles, independent but close together, are used to obtain the magnitude and direction of the surface-shear-stress vector. In principle, this device relies only on the universality of the velocity profile in the viscous sublayer, and not on the logarithmic law.

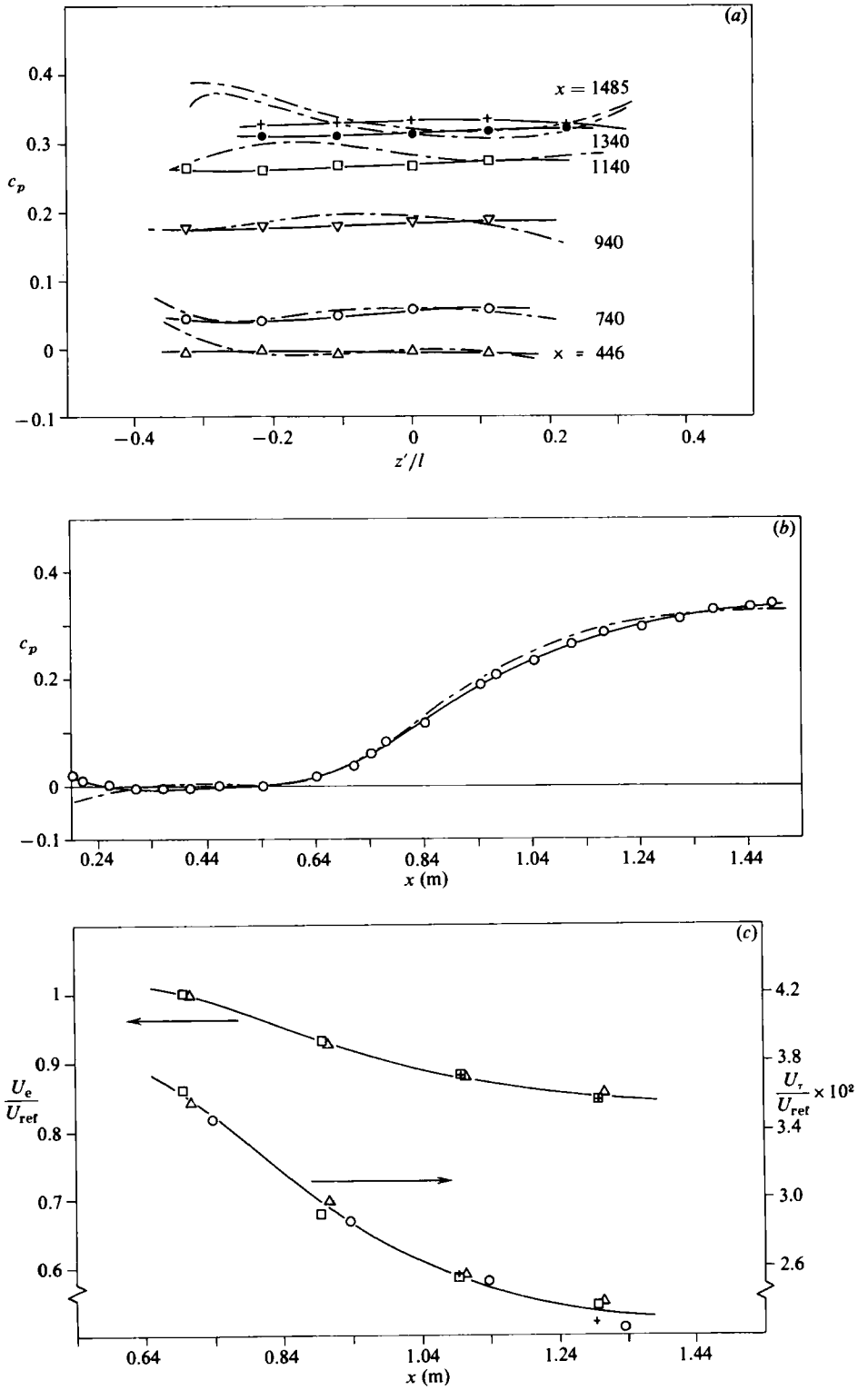

FIGURE 2 (*a–c*). For description see facing page.

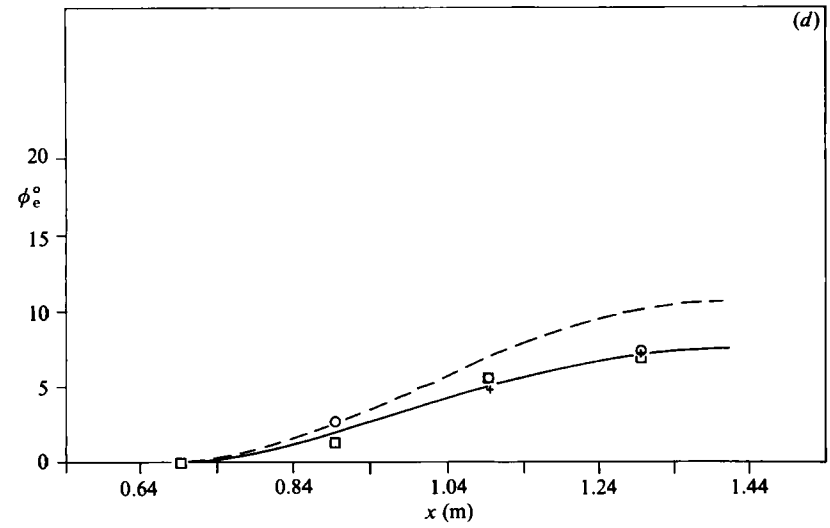

FIGURE 2. The 'external' flow: – · – · –, NLR measurements. (*a*) Surface-pressure distribution parallel to generators: z/l is distance from centreline as fraction of generator length, x is along tunnel axis, x origin at suction slot, c_p reference at $x = 466$ mm. (*b*) Surface-pressure distribution parallel to tunnel axis, in boundary-layer measurement plane. (*c*) Magnitude of boundary-layer-edge velocity U_e and friction velocity u_τ. U_{ref} is U_e at $x = 692$ mm (first measurement station). □, △, 3-hole yawmeter parallel to tunnel axis; +, 3-hole yawmeter, null reading; ○, surface-fence pair. (*d*) Direction of boundary-layer edge velocity. ×, 3-hole yawmeter; □, +, 3-hole yawmeter, null reading; ○, calculated from surface pressure assuming infinite-swept-wing conditions.

3. Physics of three-dimensional boundary layers

In two-dimensional boundary layers, a longitudinal (x-wise) pressure gradient does not directly alter the spanwise component of vorticity on a given streamline. Thus, to the boundary-layer approximation, the mean shear $\mathrm{d}U/\mathrm{d}y$ is not affected by pressure gradient, except in the 'internal layer' in which viscous and turbulent diffusion smooth out the effect of the no-slip condition at the surface. In 3D flows the response to x-wise pressure gradients is generally similar, but a z-wise component of pressure gradient leads to a velocity gradient $\mathrm{d}W/\mathrm{d}y$, that is, to streamwise vorticity. The Squire–Winter–Hawthorne (SWH) inviscid-secondary-flow formula shows that, for small disturbances, rotation of the velocity vector through an angle α to the right (positive z) rotates the mean-vorticity vector from its initial direction, parallel to the z-axis, through an angle α to the left. We shall see below that the SWH inviscid formula gives surprisingly good results for flows like the present one, in which an initially 2D boundary layer enters a region with a strong z-wise component of pressure gradient. A second-order effect of this 'skewing' of the initially z-wise vorticity vector is that the mean shear in the original (x, y)-plane $\mathrm{d}U/\mathrm{d}y$ gradually decreases. Conventional transport-equation turbulence models for the (x, y)-plane shear stress $-uv$ in a 3D boundary layer do not include $\mathrm{d}W/\mathrm{d}y$: it does not appear in the 'generation' term $v^2\,\mathrm{d}U/\mathrm{d}y$ in the exact transport equation for $-uv$, and is not normally included in models of the pressure–strain term, except as a rather small second-order effect. If the flow was initially two-dimensional the response of uv to a z-wise component of mean shear must be symmetrical, so that any formal expansion begins with a second-order term in $(\mathrm{d}W/\mathrm{d}y)^2$, but the results of the NLR experiment and the present work suggest that the effect of $\mathrm{d}W/\mathrm{d}y$ on uv is in fact quite large.

Analogously, the effect of $\mathrm{d}U/\mathrm{d}y$ on the cross-stream shear stress vw is implicitly assumed small in most calculation methods. The most obvious of the observed phenomena, the lag of the shear-stress direction $\gamma_\tau = \tan^{-1}(vw/uv)$ behind the direction of the mean-velocity gradient $\gamma_g = \tan^{-1}[(\mathrm{d}U/\mathrm{d}y)/(\mathrm{d}W/\mathrm{d}y)]$ is at least qualitatively represented by transport-equation models, because these relate the *rate of change* of shear stress, rather than the shear stress itself, to the relevant mean-velocity gradient.

A popular method of representing the crossflow-velocity profile in a 3D boundary layer is the 'triangular' plot, used by Johnston (1957; see also Johnston 1960) and attributed by him to Gruschwitz (1935), in which the velocity component perpendicular to the local free-stream direction is plotted against the velocity component in the free-stream direction. The SWH formula immediately predicts that the outer (small-defect) part of the triangular profile should be a straight line, and in the present case the slope of the outer part in the real turbulent boundary layer is close to the SWH prediction. Johnston (1960) presents an allowance for finite velocity defect but the main shortcoming of the inviscid SWH formula is that it neglects entrainment into the boundary layer.

A first approximation for the axial component of shear stress uv is that uv and the turbulent energy, both on a given streamline, should be unaffected by the axial and lateral components of pressure gradient. The 'frozen flow' approximation implies that the cross-stream component of shear stress vw remains zero in axes referred to the original two-dimensional flow. However, one expects the response of vw to $\mathrm{d}W/\mathrm{d}y$ to be of first order and, indeed, eddy-viscosity methods – which neglect flow history and 'lag' effects – simply yield $-vw$ proportional to $\mathrm{d}W/\mathrm{d}y$. Thus, in the notation introduced above, $\gamma_\tau = \gamma_g$. As commented above, current transport-equation methods qualitatively predict the lag of γ_τ behind γ_g as the latter increases in magnitude, but do not predict the decrease (or diminished increase), of uv in the presence of significant $\mathrm{d}W/\mathrm{d}y$. Specifically, even transport-equation methods do not seem to predict the observed decrease in the parameter a_1, equal to (shear-stress magnitude)$/(u^2+v^2+w^2)$.

Clearly, the influence of $\mathrm{d}W/\mathrm{d}y$ on uv implies that the larger, shear-stress-producing, turbulent eddies in an initially 2D boundary layer tend to become less organized if they are tilted over in the (y, z)-plane by the lateral mean shear $\mathrm{d}W/\mathrm{d}y$. This effect shows up most clearly when an initially 2D boundary layer is perturbed, but presumably occurs whenever the direction of the mean-velocity-gradient vector is changing downstream. We seek the explanation in the behaviour of the pressure–strain terms in the shear-stress transport equations. Our empirical attempts to represent the effect of a streamwise rate of change of γ_g on the shear stress are described below.

Finally, it should be noted that the customary resolution of the shear stress and/or the eddy viscosity into components along, and perpendicular to, the direction of the mean-velocity vector is highly confusing because this direction is not translationally invariant, as pointed out in the review of turbulence modelling in §1. The meaningful directions in the flow are those of the resultant velocity gradient, the vector whose components are $(\mathrm{d}U/\mathrm{d}y, \mathrm{d}W/\mathrm{d}y)$, or the shear-stress vector whose components are $(-uv, -vw)$. On the other hand, most of the results presented below are resolved with respect to the tunnel axis, the original direction of the flow: this does not imply that general turbulence models should use such axes, but it is legitimate and informative to treat the present flow as a 3D perturbation of an initially 2D boundary layer.

4. Results and discussion

The mean-velocity and Reynolds-stress measurements presented here are not intended as replacements for those of the NLR experiment, although the substantial corroboration of the NLR measurements has some value. The present measurements are a self-contained set, including measurements of triple products and some higher-order statistics.

Measurements were made at a number of lateral positions along the initial generator as a check that the initial boundary layer was 'two-dimensional', the quotes being inserted because what is actually required is a boundary layer with its origin on a line swept at 35°: past measurements generally indicate that leading-edge sweep, as such, has a negligible effect on both the growth rate and other characteristics of a boundary layer in zero pressure gradient, as one would expect from the boundary-layer approximation. The main set of measurements was taken at four stations on a line parallel to the tunnel axis (figure 1). The difference between this and measurements on a line perpendicular to the generators in plan view (the x'-direction in figure 1) is negligible if infinite-swept-wing conditions have really been achieved.

The pressure rise and crossflow angle upstream of the first measurement station were fairly small, the free-stream deflection at the first station being less than 1°, compared with 4° in the NLR experiment, which simplifies analysis of the results. Details of the checks at the initial generator, and of the results in general, are given by Pontikos (1982).

Figure 3 shows the mean-velocity-magnitude profiles at the four streamwise stations, and figure 4 shows the corresponding profiles of crossflow angle, measured relative to the local velocity at the edge of the boundary layer. Values of the traditional integral parameters for the four stations are given in table 1, and the increase of shape parameter H_{11} shows the effect of the pressure gradient on the velocity component in the free-stream direction. Figure 5 shows the Johnston 'triangular' or 'polar' plot of the velocity components, resolved with respect to the free-stream direction and normalized by the local free-stream velocity. The straight-line fits to the outer part of the profiles are in fact deductions from the SWH inviscid formula with the measurements at $x = 692$ mm as a starting point, and are seen to fit the results quite well. This is partly a coincidence, because the mass-flow rate in the boundary layer increases by a factor of nearly three between the first and last stations, but it certainly indicates that the 3D flow is 'pressure driven' rather than 'shear driven'. As usual, the peak of the triangular plot corresponds to a position well down in the viscous sublayer: this underestimates the actual thickness of the 'internal layer'. The lines radiating from the origin in figure 5 have slopes equal to the tangents of the surface crossflow angles, measured with the surface fence. There is obviously a discrepancy with the yawmeter measurements, but excellent agreement was obtained between the surface fence and the yawmeter when the latter was touching the surface *if* the yawmeter was calibrated on the surface (below a two-dimensional boundary layer): the discrepancy near the surface in figure 5 is entirely due to wall effect on the yawmeter when used in non-nulling mode with the 'free-stream' calibration. Figure 6 shows the magnitude and direction of the surface shear stress. Here, the surface-shear-stress direction or 'limiting streamline angle' is referred to the tunnel axis rather than to the local free stream: 'separation', that is, zero component of surface shear stress normal to the generators, occurs when the wall-flow angle reaches 55° (90° minus sweep angle) but the shear-stress magnitude, obviously equal at this point to the component along the generators, is not zero. The

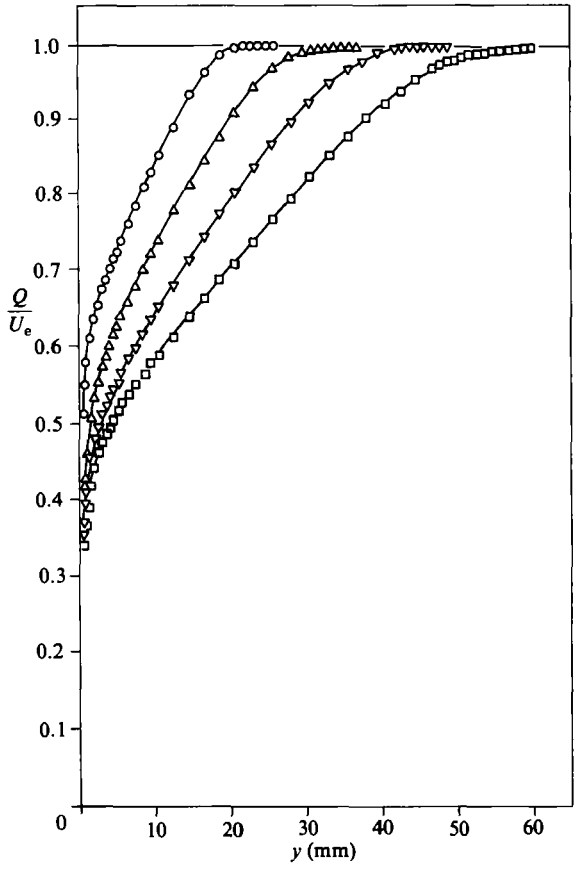

FIGURE 3. Magnitude of velocity in boundary layer. ○, $x = 692$ mm, $U_e/U_{e,ref} = 1$; △, 892, 0.932; ▽, 1092, 0.881; □, 1292, 0.847.

present experiment remains well short of separation, in contrast to the NLR experiment whose results are shown for comparison.

Figure 7 shows Reynolds stresses at the four streamwise measurement stations, again resolved with respect to the tunnel axis and not the local free-stream direction as is more usual. Figure 7 (*g*) shows the turbulent-energy profiles which are of course independent of the axes chosen. Figure 7 (*h*) shows the ratio of the shear-stress magnitude to (twice) the turbulent energy, which decreases very significantly as the crossflow increases, as in the NLR experiment. The decrease of a_1 near the surface is found even in 2D boundary layers in an adverse pressure gradient, because the shear stress is reduced near the surface while the intensity still receives significant contributions from irrotational disturbances induced by pressure fluctuations generated in the outer layer.

The individual Reynolds-stress profiles in figure 7 are not qualitatively noteworthy, except for the behaviour of vw. This is the component of shear stress normal to the direction of the original 2D boundary layer, and it rises remarkably slowly in response to the imposed cross-stream shear-velocity gradient $\mathrm{d}W/\mathrm{d}y$. The present measurements did not extend into the inner layer, where vw necessarily changes more rapidly because the resultant shear-stress direction asymptotes to that of the limiting

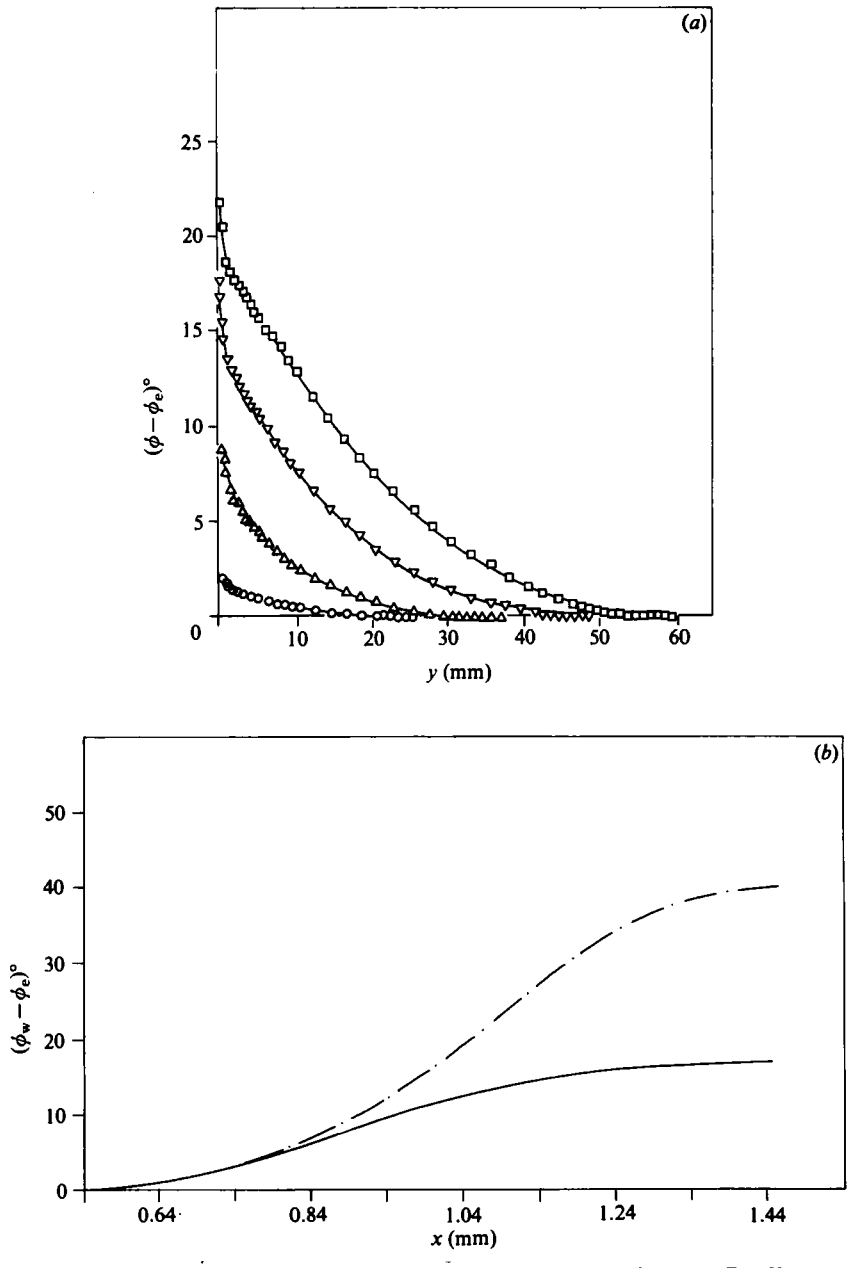

FIGURE 4. Direction of velocity in boundary layer, relative to edge. (*a*) Profiles ○, $x = 692$, $\phi_e = 0.03°$; △, 892, 1.43°; ▽, 1092, 5.54°; □, 1292, 7.02°. (*b*) ——, Wall values; and – – –, NLR results.

streamline at the surface. The scatter in the hot-wire measurements of vw is attributable to their deduction as the small difference of large quantities: the same scatter in, say, v^2 would be scarcely noticeable as a percentage.

The best overall view of the shear-stress direction is provided by figure 8, which shows the directions of the mean velocity, mean-velocity gradient and resultant shear stress. The tradition for such plots (Bradshaw & Terrell 1969; Johnston 1970) is to

x, mm	U_e, ms^{-1}	ϕ_e°	ϕ_w°	u_τ, ms^{-1}	$c_f \equiv 2(u_\tau/U_e)^2$
692	33.7	0.03	2.3	1.19	0.00251
892	31.4	1.43	10.0	1.03	0.00213
1092	29.7	4.89	18.5	0.871	0.00172
1292	28.6	7.18	24.6	0.775	0.00147
x, mm	δ_{995}, mm	δ_{11}^*, mm	θ_{11}, mm	$H_{11} \equiv \delta_{11}^*/y_{11}$	
692	20.0	3.43	2.50	1.37	
892	29.3	5.89	4.04	1.46	
1092	41.5	9.10	5.94	1.53	
1292	53.8	12.69	7.99	1.59	

TABLE 1. External-stream and boundary-layer parameters. Figure 4(*b*) shows smooth curve through $\phi_w - \phi_e$.

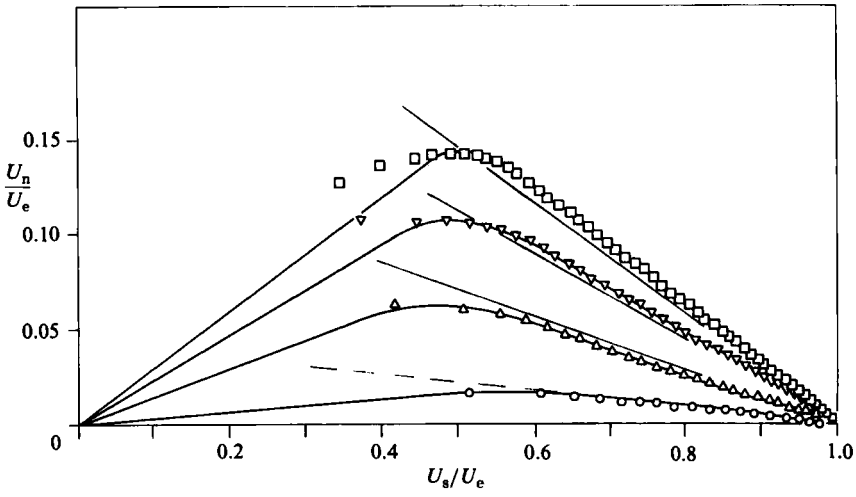

FIGURE 5. Johnston polar plot of velocity in boundary layer. U_s, component parallel to edge streamline; U_n, component normal to edge streamline. Symbols as in figure 4.

refer them to the local free-stream direction: figure 8, following van den Berg (Fernholz 1982), shows the tunnel-axis direction so that the total deflection of the shear-stress vector can be seen at a glance. The tangents of the velocity-gradient and shear-stress angles tend to 0/0 at the boundary-layer edge and are therefore unreliable, but the overall trend in the outer layer shows a very slow response to the application of the cross-stream velocity gradient. The more rapid response in the inner part of the outer layer (e.g. $y < 10$ mm at $x = 1092$ mm) is perhaps only marginally significant in view of the likely experimental errors. The simplest way of expressing the results is to say that at $x = 1292$ mm the shear-stress direction in the main part of the boundary layer has turned through only about one-third of the angle through which the velocity-gradient vector has turned from its original direction along the tunnel axis. Note that this is not a rapidly distorted flow: the distance between the start of crossflow ($x = 540$ mm) and the last measurement station at $x = 1292$ mm is over forty times the boundary-layer thickness at the start of crossflow. Quantities such as eddy viscosities, ratios of Reynolds stresses, etc., are given by Pontikos (1982).

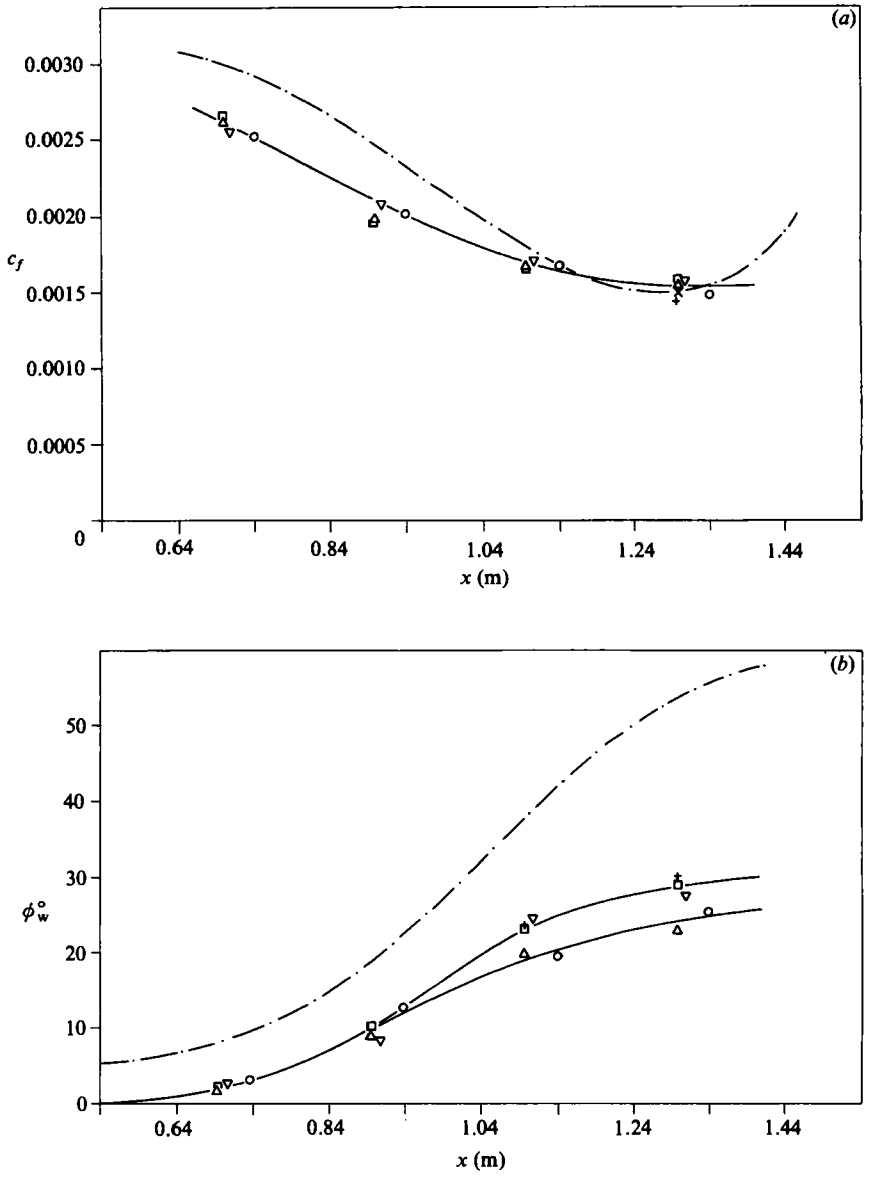

FIGURE 6. Skin friction coefficient, $|\tau_w|/\frac{1}{2}\rho U_e^2$, and direction of τ_w relative to tunnel (x) axis. ○, surface-fence pair; other symbols, 3-hole yawmeter (log-law fits and 'Preston-tube' calibration); – · – · –, NLR results. (*a*) c_f magnitude; (*b*) direction of τ_w.

The main new contribution of the present work is a complete set of triple-product measurements, which are plotted by Pontikos (1982) for two sets of axes: 'tunnel' axes, with x along the tunnel centreline and z spanwise, and axes aligned with the *local* mean-velocity direction (denoted by suffix m). The latter axes are those used by the NLR group, but the former are definitely preferable in discussing perturbations of the flow from its original 2D state. Here we present only a few sample results, for Reynolds-stress transport normal to the surface.

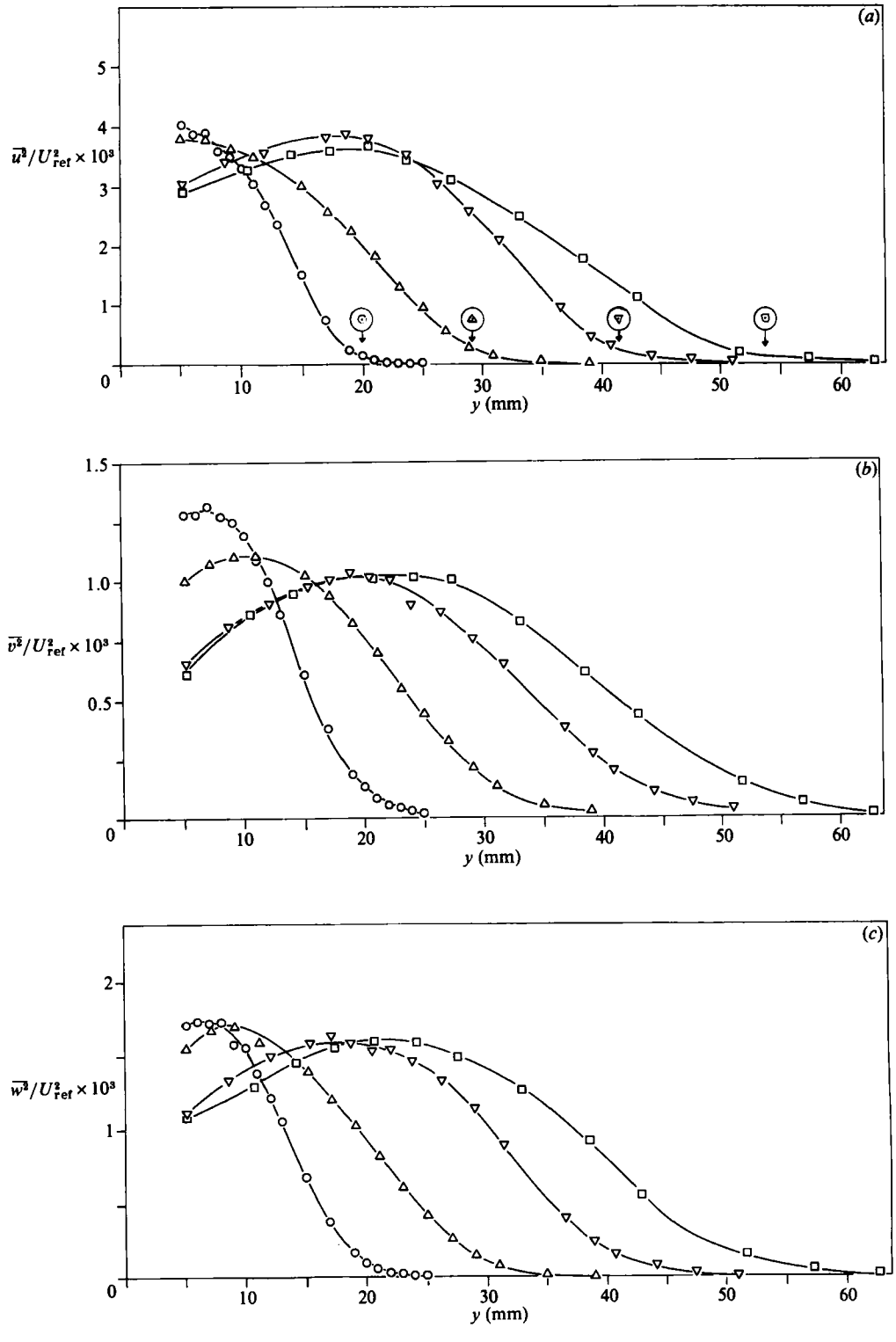

FIGURE 7 (a–c). For description see p. 120.

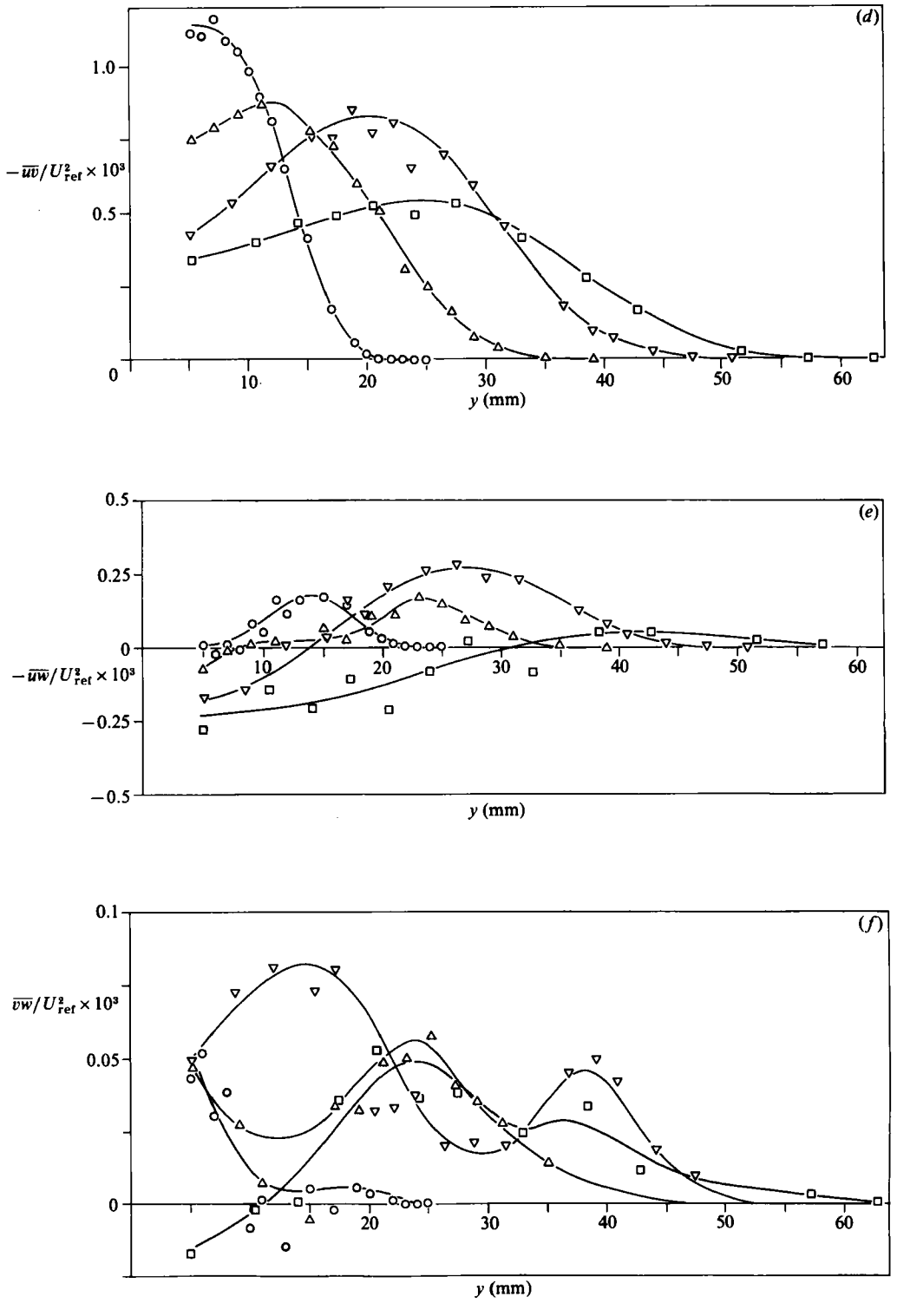

FIGURE 7(*d–f*). For description see p. 120.

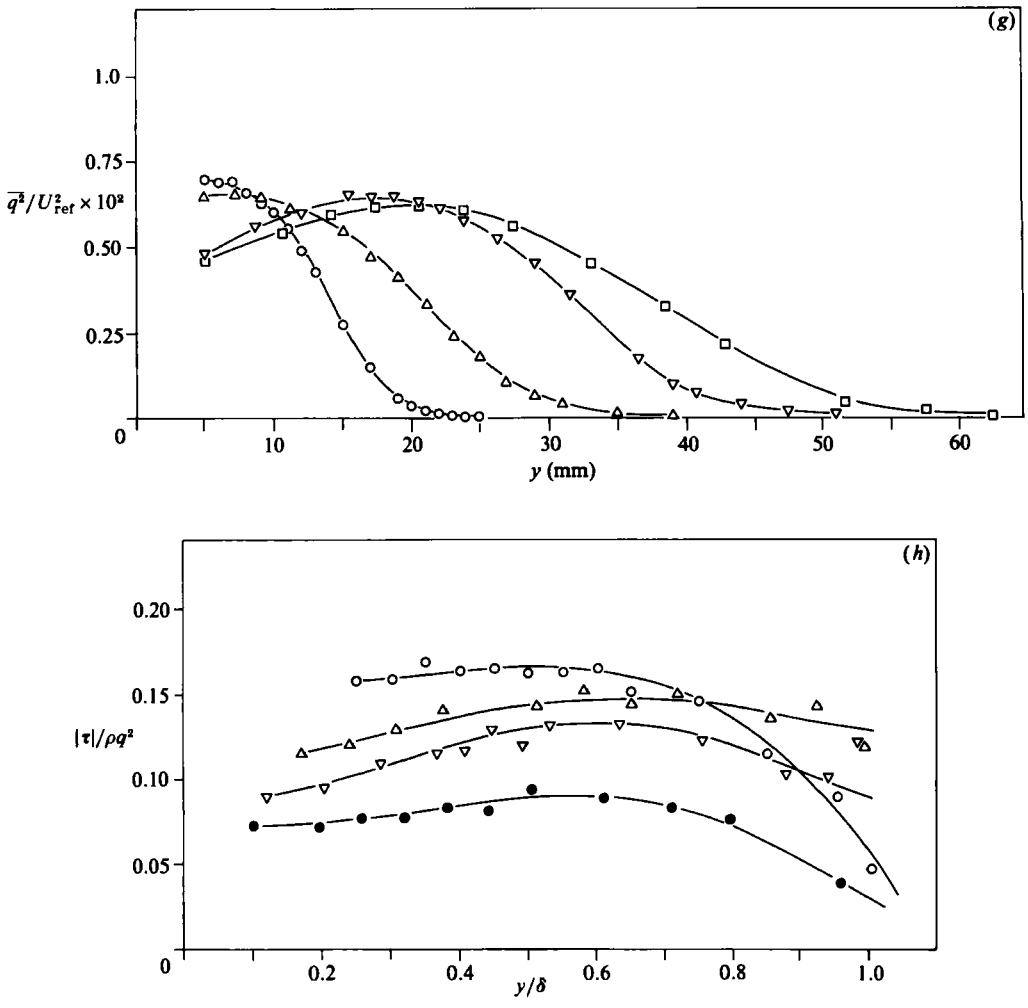

FIGURE 7. Reynolds stresses, referred to (x, z)-axes along and normal to tunnel centreline, made dimensionless with edge velocity at $x = 692$ mm, U_{ref}. Shear stresses are plotted so that the 'expected' values are positive. Symbols with arrows denote boundary-layer thickness, δ_{995}. ○, $x = 692$ mm; △, 892 mm; ▽, 1092 mm; □, 1292 mm. (*a*) $\overline{u^2}/U_{ref}^2$, (*b*) $\overline{v^2}/U_{ref}^2$, (*c*) $\overline{w^2}/U_{ref}^2$, (*d*) $-\overline{uv}/U_{ref}^2$, (*e*) $-\overline{uw}/U_{ref}^2$, (*f*) $+\overline{vw}/U_{ref}^2$, (*g*) (twice) turbulent energy, $q^2 \equiv \overline{u^2}+\overline{v^2}+\overline{w^2}$, (*h*) ratio of shear-stress magnitude, $|\tau| = ((\overline{uv})^2+(\overline{vw})^2)^{\frac{1}{2}}$, to twice turbulent energy, $q^2 = \overline{u^2}+\overline{v^2}+\overline{w^2}$.

Figure 9(*a*) shows the y-component transport velocity for the turbulent kinetic energy, defined as

$$V_q = \frac{\overline{u^2v}+\overline{v^3}+\overline{w^2v}}{\overline{u^2}+\overline{v^2}+\overline{w^2}}, \tag{2}$$

where the unmeasurable pressure contribution is neglected. In 2D boundary layers, the ratio of V_q to the free-stream velocity, if not the absolute value of V_q, tends to rise in regions of adverse pressure gradient as the relative turbulence intensity increases. (The same applies to the eddy diffusivity of turbulent kinetic energy.) In the present boundary layer V_q decreases strongly with x as the result of a strong decrease in the raw triple products. V_q becomes negative near the surface, as in 2D

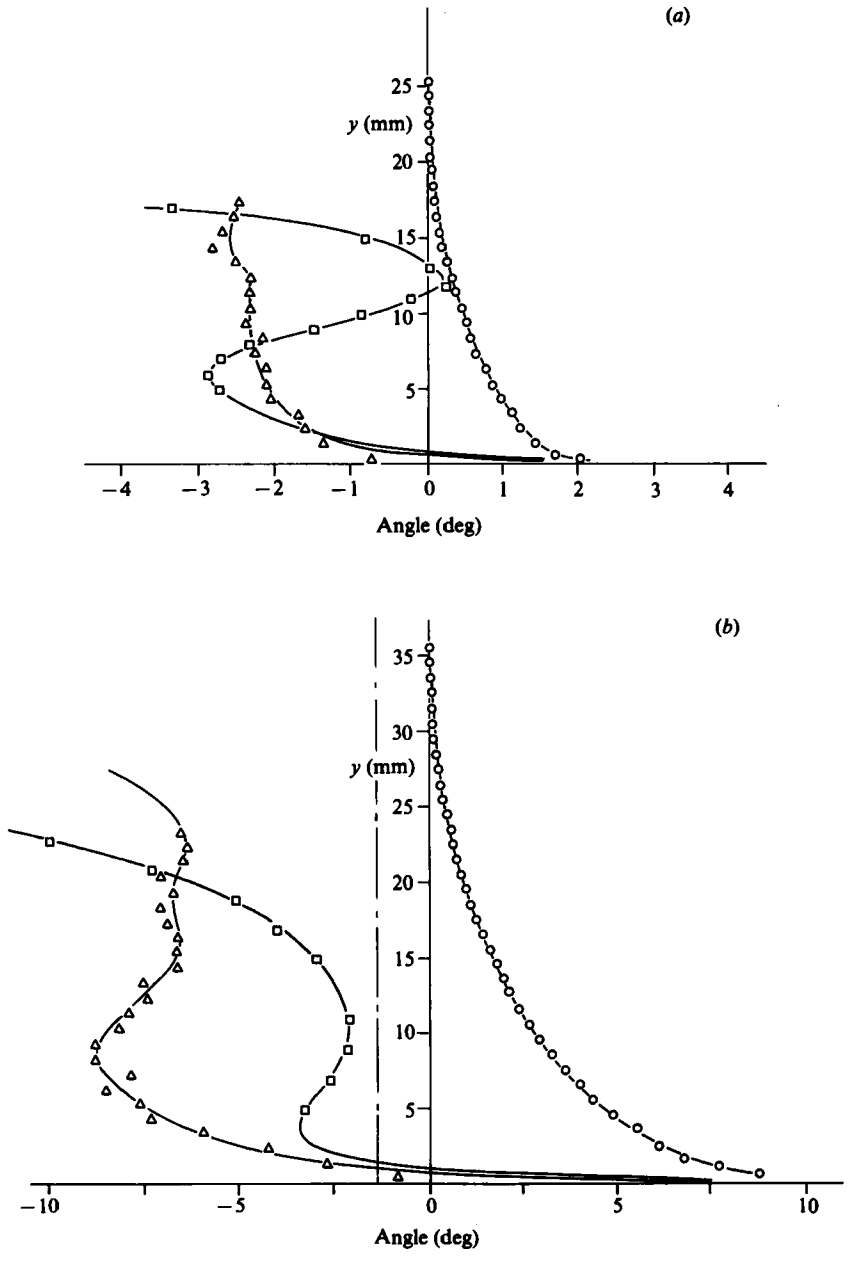

FIGURE 8(*a–b*). For description see next page.

boundary layers in strong adverse pressure gradient. Figure 9(*b*) shows the transport velocity for the component of shear stress along the tunnel axis, defined as

$$V_{uv} = \frac{\overline{uv^2}}{\overline{uv}}. \tag{3}$$

This tends to 0/0 at the edge of the boundary layer more quickly than V_q, and values in the outermost part of the layer are therefore uncertain. However, the absolute

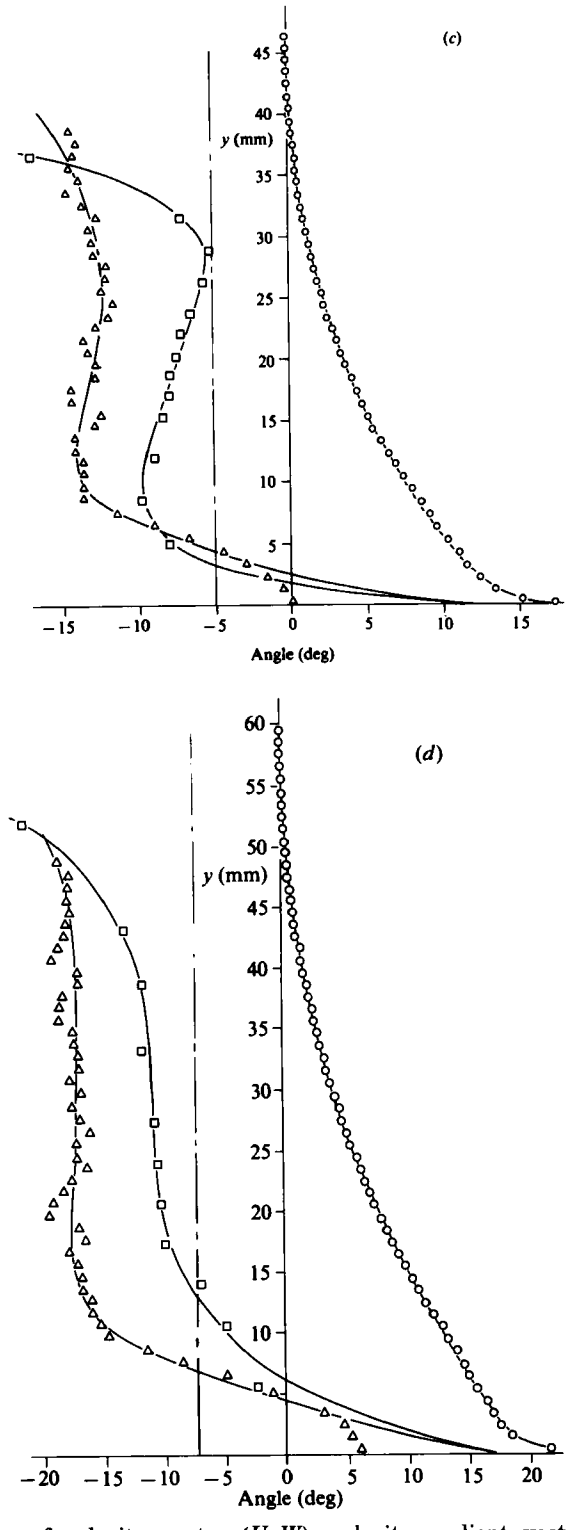

FIGURE 8. Direction of velocity vector (U, W), velocity-gradient vector $(\partial U/\partial y, \partial W/\partial y)$ and shear-stress vector $(-\overline{uv}, -\overline{vw})$ with respect to the external streamline. ○, velocity; △, velocity gradient; □, shear stress; – · – · – · –, tunnel-axis direction. (*a*) x = 692 mm, (*b*) 892 mm, (*c*) 1092 mm, (*d*) 1292 mm.

value of V_{uv} at $y/d = 0.75$ is seen to decrease slightly over the first three stations, with a small rise at the fourth station. Again as in 2D boundary layers in adverse pressure gradients, negative values appear near the surface. Figure 9(*c*) shows the triple product in the numerator of V_{uv}, and figure 9(*d*) shows the triple product in the numerator of the transport velocity of the cross-stream component of shear stress, defined as

$$V_{vw} = \frac{\overline{v^2 w}}{\overline{vw}}. \tag{4}$$

Figure 9(*c*) shows that uv^2 simply decreases with downstream distance, as implied by the plot of V_{uv}. However, v^2w at first decreases with increasing downstream distance in much the same way as uv^2, but collapses almost entirely at the last station, with the exception of large and scattered values near the surface. This quantity is extremely difficult to measure, but the only reason why results at the last station should be particularly unreliable is that the crossflow velocity over the probe is largest there – although the yaw angle in the outer layer at the last station is no larger than the angle in mid-layer at the preceding station, where the v^2w measurements seem to be following the same trend as uv^2.

The general conclusions from the triple-product measurements are: that the ability of the large eddies to 'diffuse' turbulent energy – that is, to transport it in the y-direction – is significantly reduced by the onset of three-dimensionality; that the same applies to the diffusion of the component of shear stress along the original flow direction; but that the diffusion of the new, cross-stream component of shear stress collapses as the crossflow becomes large. Another case in which the triple products collapse is the centrifugally stabilized flow over a convex surface (e.g. Smits, Young & Bradshaw 1979): in this case, the Reynolds stresses also collapse, but recover more rapidly than the triple products.

Figure 10 shows the turbulent-kinetic-energy balance conventionally plotted with a gain of kinetic energy (e.g. from production) shown as negative. Viscous dissipation of turbulent energy has been obtained as the sum of all the other terms, including experimental error and the neglected pressure diffusion. The general behaviour is similar to that of 2D boundary layers in adverse pressure gradients, but the 'measured' dissipation rate is consistently larger than the prediction of the empirical formula

$$\epsilon = \frac{(|\tau|/\rho)^{\frac{3}{2}}}{0.1\delta}, \tag{5}$$

which works well both in wholly 2D flows and at the upstream station in the present flow. The consequence of this extra dissipation is the downstream decrease of turbulent energy already noted, and it is evidently one of the keys to the anomalous behaviour of 3D boundary layers. Pontikos gives balances for the three components of shear stress, resolved for convenience in axes along and normal to the generators. (Serious use of the data would require tabulations so we do not give graphs here.) As in 2D flow, generation of shear stress by interaction between the existing turbulence and the mean flow is almost balanced by pressure–strain 'redistribution' or 'scrambling', otherwise known as the 'return-to-isotropy' term. Transport terms are comparatively small, so the shear-stress balances are not qualitatively spectacular, although the excess of pressure–strain redistribution over generation is the root cause of decrease of the shear-stress magnitude, just as the excess of dissipation over production explains the decay of turbulent energy.

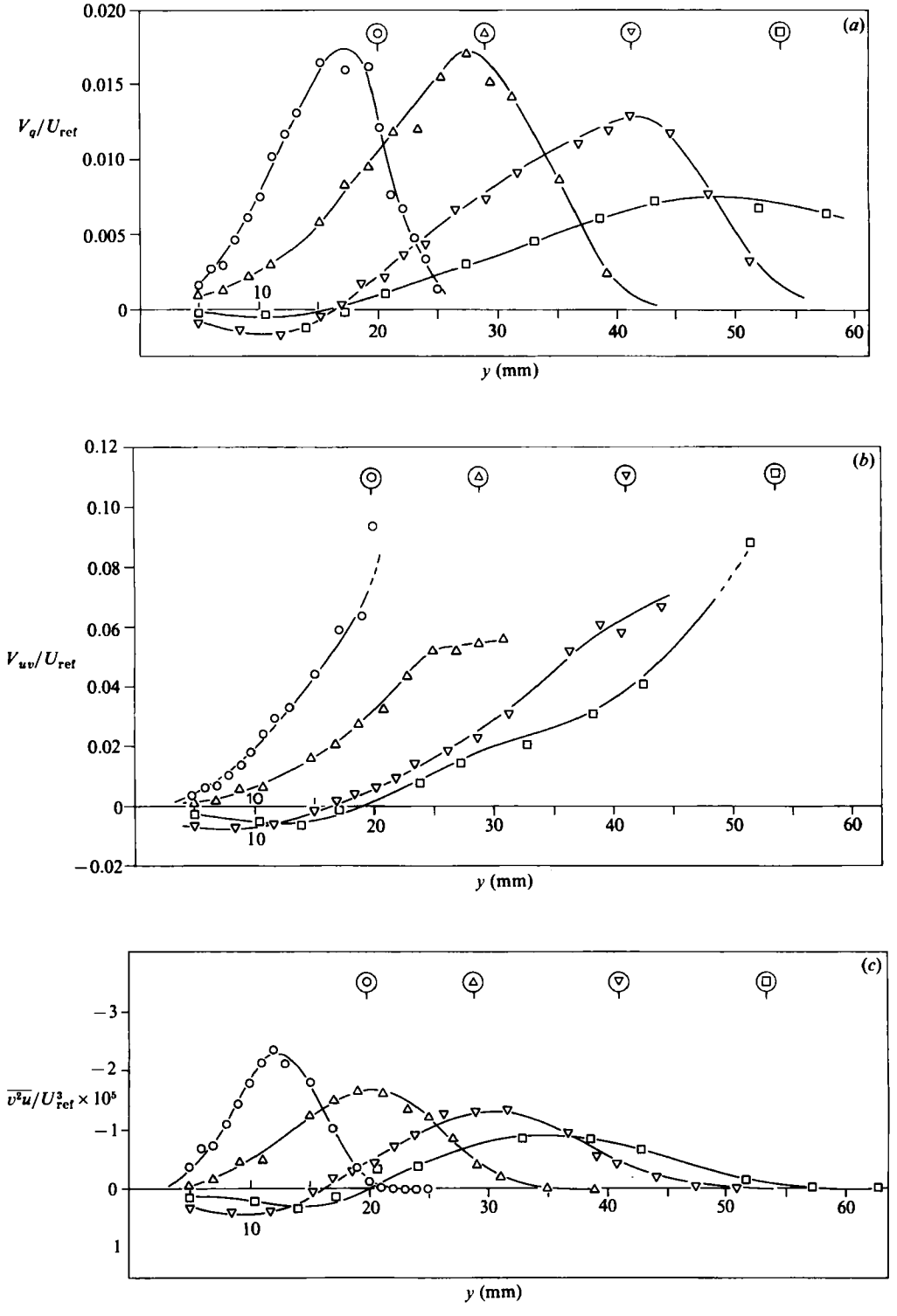

FIGURE 9(*a–c*). For description see facing page.

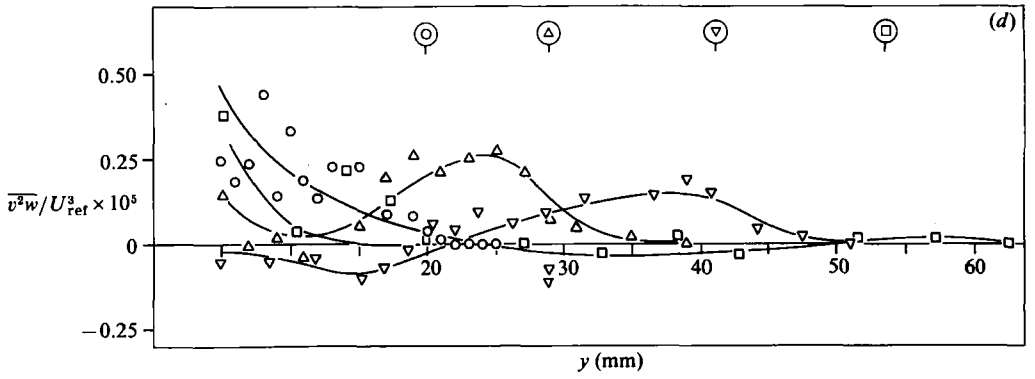

FIGURE 9. Triple products. (*a*) *V*-component transport velocity of turbulent energy by triple products, $V_q = \overline{q^2 v}/\overline{q^2}$. (*b*) *V*-component transport velocity of axial shear stress $-\overline{uv}$ by triple products, $V_{uv} = \overline{uv^2}/\overline{uv}$. (*c*) Triple product $\overline{uv^2}$ appearing in V_{uv}. (*d*) Triple product $\overline{v^2 w}$ appearing in V_{vw}.

Fourth-order products have also been measured and the v-component flatness factor is shown in figure 11. As usual, values in the inner part of the boundary layer are slightly below the Gaussian value of 3, while the peak values increase slightly with x, ending with a decrease at the last station. The u-component flatness factor (not shown here) actually reaches a slightly higher peak value at the last station, while the w-component flatness factor, which reaches peak values of as much as 30 in the outer part of the boundary layer at the first three stations, decays to a peak value not much more than 20 at the last station. A remarkable feature shared by all three flatness factors is that the region with roughly the 'Gaussian' value of 3 extends further and further out, as a fraction of the peak location, as the boundary layer becomes more three-dimensional. Figure 12 shows the intermittency, the presence of turbulence being equated to the presence of large first or second time derivatives of uv. Like any other criterion based on the velocity-fluctuation field, this fails to give a maximum intermittency of unity unless forced to do so because short quiescent intervals inside the turbulence are inevitably recorded as non-turbulent. However, it is clear that there is only a slight trend in the intermittency; the flank of the profile moves slightly further out relative to the boundary-layer thickness as the flow becomes more three-dimensional. Since the boundary-layer thickness is just a record of the history of the shear-stress gradient near the outer edge of the boundary layer, it is if anything less representative of the scale of the turbulent region than, say, the distance from the surface at which the intermittency falls to 0.5: one should not, therefore, make too much of the trend in figure 12, although a crude equation of the intermittency to 3/(flatness factor), exact for an on–off Gaussian process, is consistent with a decrease in peak flatness factor near the outer edge of the boundary layer at the later stations.

5. General discussion and conclusions

Although the measurement of cross-statistics involving both the v- and w-component fluctuations is subject to considerable uncertainty, the present results for a simulated 'infinite' swept wing show a consistent picture. Turbulent activity decreases as the flow becomes more three-dimensional, leading to reductions in the 'diffusion' (rate

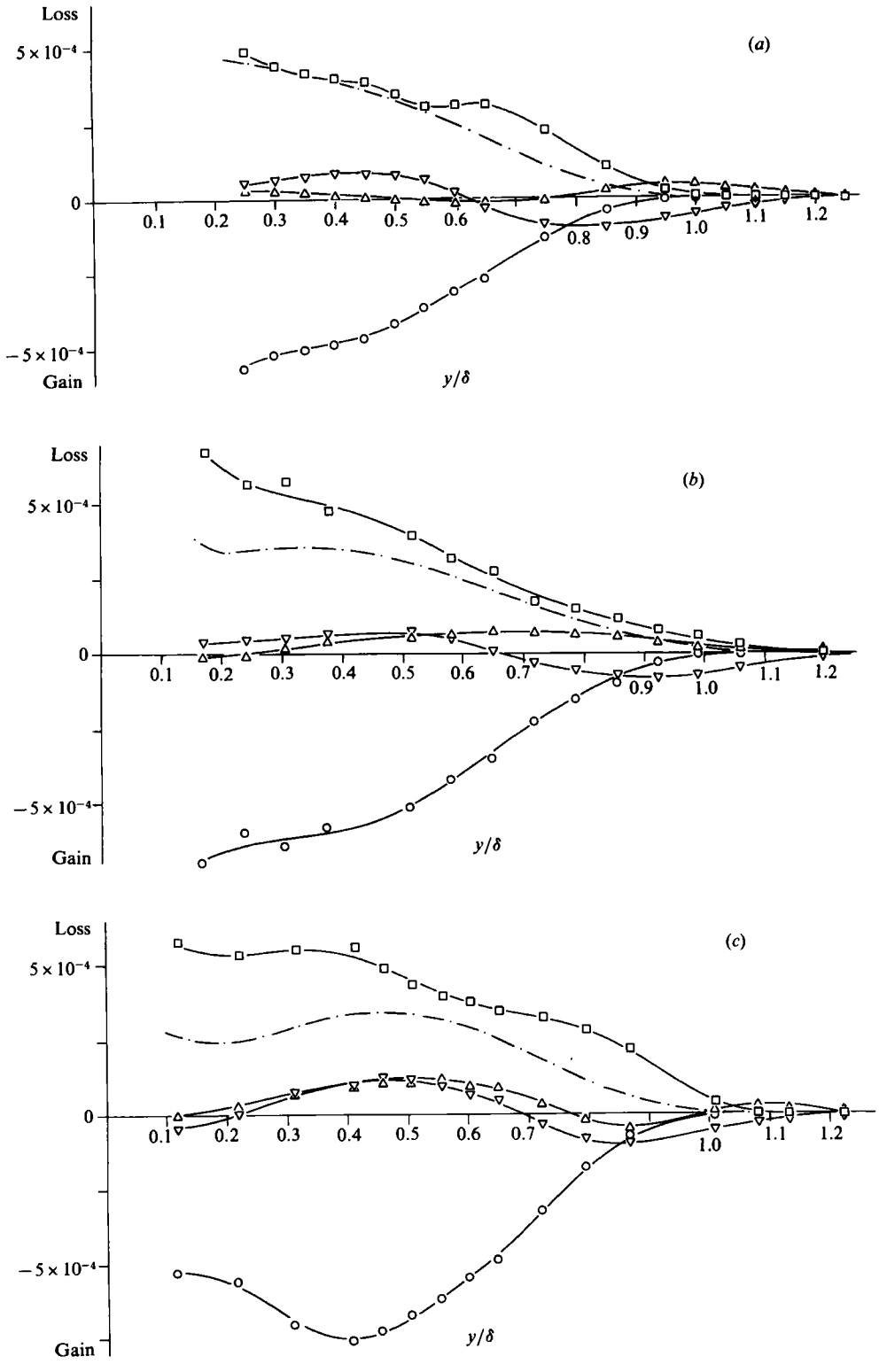

FIGURE 10(*a–c*). For description see facing page.

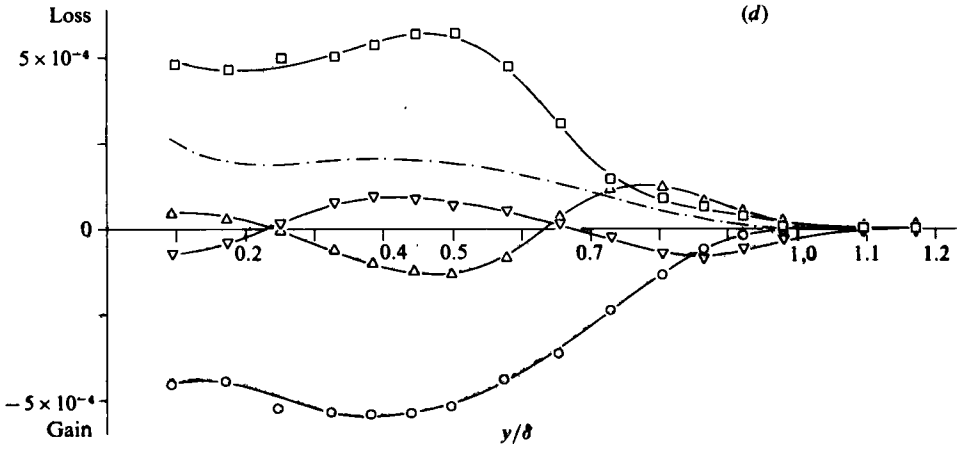

FIGURE 10. Turbulent-energy balances. ○, production; △, advection (transport by mean flow); ▽, diffusion (transport by turbulence); □, dissipation (difference of other terms); – · – · –, dissipation (from empirical formula (5) for two-dimensional flows). All terms made dimensionless by local free-stream velocity U_e and boundary-layer thickness δ_{995}. (*a*) $x = 692$ mm, (*b*) 892 mm, (*c*) 1092 mm, (*d*) 1292 mm.

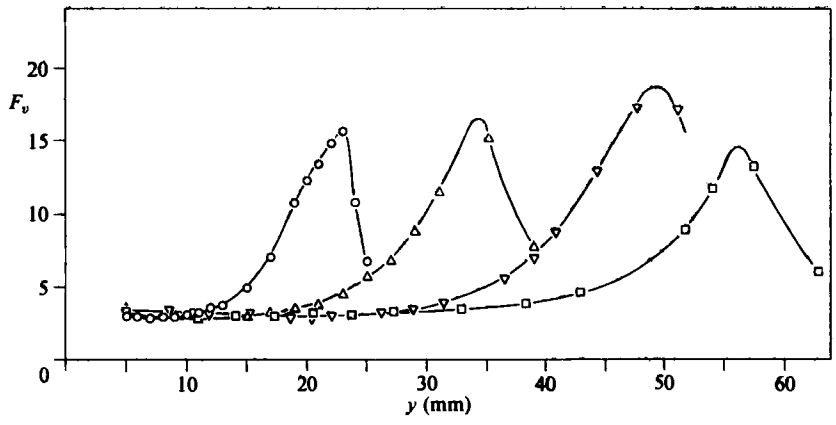

FIGURE 11. v-component flatness factor, $F_v = \overline{v^4}/(\overline{v^2})^2$.

of transport, normal to the surface) of momentum, turbulent energy, and shear stress. The data analysis did not include detailed conditional sampling, signal-pattern recognition or other techniques for exploring the details of eddy structure. However, it is clear that the application of a spanwise velocity gradient $\mathrm{d}W/\mathrm{d}y$ to an initially 2D flow driven by a velocity gradient $\mathrm{d}U/\mathrm{d}y$ strongly affects the behaviour of the large eddies which effect most of the turbulent transport. If $\mathrm{d}W/\mathrm{d}y$ rose from zero to a fixed proportion of $\mathrm{d}U/\mathrm{d}y$, the large eddies and the shear-stress vector would eventually align themselves along the new direction of the resultant velocity gradient, and relax to the structure typical of 2D flows: it is the *rate of change* of $\mathrm{d}W/\mathrm{d}y$ that affects the eddy structure. The simplest hypothesis is that the large eddies are 'tilted' sideways by $\mathrm{d}W/\mathrm{d}y$. If one regards the statistical average shape of the large eddies as a sort of eigenmode or preferred disturbance shape, it follows that the large eddies in a 2D flow are the most efficient structures for extracting kinetic energy from the

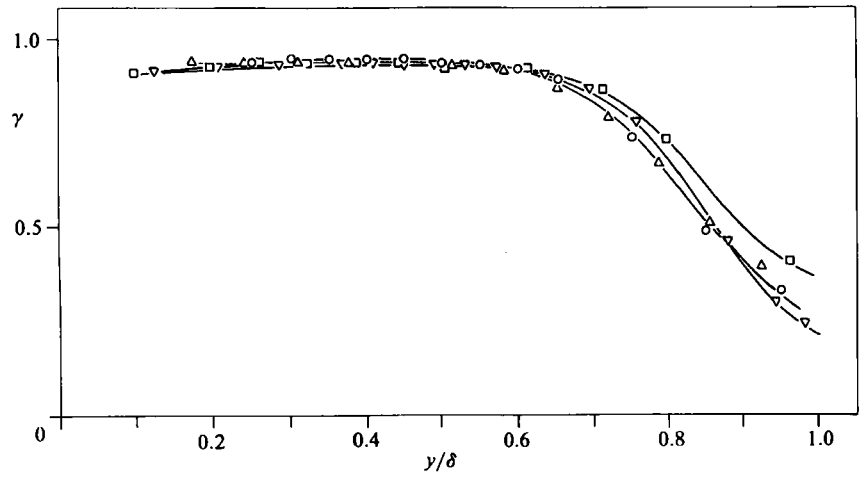

FIGURE 12. Intermittency factor γ (from first and second time derivatives of uv).

mean shear $\mathrm{d}U/\mathrm{d}y$, that is, the most efficient producers of shear stress. It seems plausible that tilting the large eddies over sideways will confuse their behaviour and reduce their efficiency (say, the stress-energy ratio plotted in figure 7*h*). Note that tilting through a large angle is not necessarily implied: the integral of $\mathrm{d}W/\mathrm{d}y$ in mid-layer down the length of the flow is only about 30°. In boundary layers with imbedded longitudinal vortices (e.g. Shabaka, Mehta & Bradshaw 1985) tilting through angles of order 90° *can* occur, so that the new uv comes mainly from the old uw – which is of course zero in an initially two-dimensional flow. However in ordinary 3D boundary layers the effect of crossflow or tilting must be more subtle.

A speculative model of the effect of tilting has been explored by Mr A. J. Davies (undergraduate project at Imperial College) and the authors. The 'destruction' terms in a transport-equation turbulence model are increased by an amount proportional to a fading-memory integral of the 'rate of tilt' $\mathrm{d}W/\mathrm{d}y$ along a streamline. A reduction in the streamwise component of shear stress can of course be simulated, but since the correction must be independent of the sign of the tilting and therefore goes as $(\mathrm{d}W/\mathrm{d}y)^2$ the correction tends to be too large and too late. This feature is shared by the eddy-viscosity anisotropy correction of Rotta (1977), but it should be noted that the present model exhibits correct translational invariance, unlike models based on the direction of the velocity vector which, illegally, depends on the relative velocity flow and the axis.

The broad conclusion is that the present experiment, using a configuration similar to that used in the work at NLR (van den Berg *et al.* 1975; Elsenaar & Boelsma 1974) confirms and extends the results of the latter. We have shown in greater detail that the influence of mean-flow three-dimensionality on the dimensionless structure parameters of the turbulence is more extensive and more subtle than assumed in current calculation methods, which concentrate on the lag in direction of the shear-stress vector while not fully accounting for the decrease in magnitude implied by figure 7(*h*). This influence is shown most clearly by experiments like the present one, in which an initially two-dimensional boundary layer enters a region of crossflow. The triple products that represent turbulent transport of Reynolds stress and turbulent energy normal to the surface are also affected anomalously by three-dimensionality. Evidently the addition of a 'spanwise' mean-shear component

dW/dy to a two-dimensional mean shear dU/dy distorts the eddies created by the latter so as to reduce their contribution to shear stress. A turbulence-model modification, based on the simple idea that the large eddies topple over sideways, did not reproduce the experimental results very convincingly; but this may be the fault of an over-crude representation of the toppling process rather than a fault in the basic idea.

Further work should be done on simple configurations, like the present simulation of an infinite swept wing, but should include more advanced investigations of large-eddy structure. Since most practical flows are three-dimensional, even basic turbulence research should pay some attention to the changes in eddy structure that are evidently caused by three-dimensionality of the mean flow.

We are grateful to Dr V. Baskaran for helpful comments on a draft of this paper, and for checking the surface-crossflow measurements of figure 4(*b*).

REFERENCES

BERG, B. v. D., ELSENAAR, A., LINDHOUT, J. P. F. & WESSELING, P. 1975 Measurements in an incompressible three-dimensional turbulent boundary layer under infinite swept-wing conditions, and comparison with theory. *J. Fluid Mech.* **70**, 127.

BRADSHAW, P. 1972 Two more low-turbulence wind tunnels driven by centrifugal blowers. *Imperial College Aero Rep.* 72-10.

BRADSHAW, P. & TERRELL, M. G. 1969 The response of a turbulent boundary layer on an 'infinite' swept wing to the sudden removal of pressure gradient. *NPL Aero Rep.* 1305.

CEBECI, T. 1984 Problems and opportunities with three dimensional boundary layers. Presented at *AGARD Fluid Dynamics Panel meeting, Von Kármán Institute, May 1984.*

EAST, L. F. 1975 Computation of three-dimensional turbulent boundary layers. *Euromech 60, Trondheim 1975. FFA TN AE*-1211.

ELSENAAR, A. & BOELSMA, S. H. 1974 Measurements of the Reynolds stress tensor in a three-dimensional turbulent boundary layer under infinite swept wing conditions. *NLR TR* 74095U.

FANNELØP, T. K. & KROGSTAD, P. A. 1975 Three-dimensional turbulent boundary layers in external flows: a report on Euromech 60. *J. Fluid Mech.* **71**, 815.

FERNHOLZ, H. H. (ed.) 1982 *Proc. IUTAM Symp. on Three Dimensional Boundary Layers.* Springer.

GOLDBERG, U. C. & RESHOTKO, E. 1984 Scaling and modeling of three dimensional pressure driven turbulent boundary layers. *AIAA J.* **22**, 914.

GRUSCHWITZ, E. 1935 Turbulente Reibungsschichten mit Sekundärströmungen. *Ing.-Arch.* **6**, 355.

HAWTHORNE, W. R. 1951 Secondary circulation in fluid flow. *Proc. R. Soc. Lond.* A **206**, 374.

JOHNSTON, J. P. 1957 Three dimensional turbulent boundary layers. *MIT Gas Turbine Lab. Rep.* 39.

JOHNSTON, J. P. 1960 On the three dimensional turbulent boundary layer generated by secondary flow. *Trans. ASME* D: *J. Basic Engng* **82**, 233.

JOHNSTON, J. P. 1970 Measurements in a three-dimensional turbulent boundary layer induced by a swept, forward-facing step. *J. Fluid Mech.* **42**, 823.

JOHNSTON, J. P. 1976 Experimental studies in three-dimensional turbulent boundary layers. *Stanford Univ. Thermosci. Divn Rep.* MD-34 (also, *Lockheed Georgia Co. Rep.* LG77 ER 0044, 1977).

PIERCE, F. J., MCALLISTER, J. E. & TENNANT, M. H. 1983 A review of near-wall similarity models in three dimensional turbulent boundary layers. *Trans. ASME* I: *J. Fluids Engng* **105**, 251.

PONTIKOS, N. S. 1982 The structure of three dimensional turbulent boundary layers. Ph.D. thesis, Imperial College, London. (Available on microfiche from Department of Aeronautics.)

PONTIKOS, N. S. & BRADSHAW, P. 1981 Miniature pressure probe for measuring the shear stress vector in turbulent flow. *Aero. Quart.* **32**, 43.

ROTTA, J. C. 1979 A family of turbulence models for three dimensional thin shear layers. In *Turbulent Shear Flows I* (ed. F. Durst, B. E. Launder, F. W. Schmidt & J. H. Whitelaw), Springer. Also *DFVLR-AVA IB* 251-76A25 (1976).

SHABAKA, I. M. M. A., MEHTA, R. D. & BRADSHAW, P. 1985 Longitudinal vortices imbedded in turbulent boundary layers. *J. Fluid Mech.* **155**, 37.

SMITS, A. J., YOUNG, S. T. B. & BRADSHAW, P. 1979 The effect of short regions of high surface curvature on turbulent boundary layers. *J. Fluid Mech.* **94**, 209.

SQUIRE, H. B. & WINTER, K. G. 1951 The secondary flow in a cascade of aerofoils in a uniform stream. *J. Aero. Sci.* **18**, 271.